ELSEVIER

Journal of Alloys and Compounds 311 (2000) 311–316

Journal of ALLOYS AND COMPOUNDS

www.elsevier.com/locate/jallcom

Electrochemical behaviour of nanostructured $Mm(Ni,Al,Co)_5$ alloy as MH_x electrode

M. Jurczyk[a,*], W. Majchrzycki[b]

[a]*Institute of Materials Science and Engineering, Poznań University of Technology, M. Sklodowska Curie 5 Sq., 60-965 Poznań, Poland*
[b]*Central Laboratory of Batteries and Cells, Forteczna 12/14 St., 61-362 Poznań, Poland*

Received 20 June 2000; accepted 3 July 2000

Abstract

The electrochemical properties of nanocrystalline $MmNi_{3.5}Al_{0.8}Co_{0.7}$ alloy, which has the hexagonal $CaCu_5$ type structure, were investigated. This material was prepared by mechanical alloying (MA) followed by annealing and used as a negative electrode for a Ni–MH_x battery. MA process transforms the starting mixture of the elements into an amorphous phase without other phase formation. Heating the MA sample at 1020 K for 0.5 h resulted in the formation of the hexagonal $CaCu_5$-type structure. It was found that the electrodes prepared from the nanocrystalline powders had almost similar discharge capacities, compared with the negative electrode prepared from polycrystalline powders. In the annealed nanocrystalline $MmNi_{3.5}Al_{0.8}Co_{0.7}$ powders discharging capacities up to 135 mAh g^{-1} (at 160 mA g^{-1} discharge current) were measured (note, that the lanthanum content in mischmetal was only 25 wt%).

Keywords: Electrochemical properties; Nanocrystalline; $Mm(Ni,Al,Co)_5$ alloy; Nickel–metal hydride battery

1. Introduction

The alloys of TiFe, ZrV_2 and $LaNi_5$ are familiar materials which absorb large quantities of hydrogen under mild conditions of temperature and pressure [1–5]. Among the three types of hydrogen forming compounds, $LaNi_5$-based intermetallics have recently proven to be very attractive as negative electrode material in rechargeable nickel–metal hydride batteries (Ni–MH_x) [3,6]. Unlike the conventional lead acid and nickel cadmium batteries, metal hydride batteries have a much lower content of environmentally toxic metals. The hydrogen storage materials combine a high reversible energy storage capacity with fast electrochemical activation, excellent long term cycling stability and good charge discharge kinetics, making Ni–MH_x batteries nowadays a serious alternative for Ni–Cd batteries. The Ni–MH_x battery is a battery with a hydrogen storage alloy as its negative electrode, which is able to absorb and desorb reversibly a large amount of hydrogen at room temperature. The working principle of this battery is expressed by the following equation [7]:

$$Ni(OH)_2 + M \underset{\text{discharge}}{\overset{\text{charge}}{\leftrightarrow}} NiOOH + MH_x,$$

where M stands for the hydrogen storage alloy and MH_x for metal hydride. The nickel–metal hydride battery has the following advantages [7]. The cell voltage is almost the same as the value of a Ni–Cd battery, i.e. 1.2–1.3 V. The cell can be charged and discharged at high rates and low temperatures.

The properties of hydrogen host materials can be modified substantially by alloying to obtain the desired storage characteristics, e.g. proper capacity at a favourable hydrogen pressure [3,8,9]. For example, it was found that the respective replacement of La and Ni in $LaNi_5$ by small amounts of Zr and Al resulted in a prominent increase in the cycle life time without causing much decrease in capacity. The use of an unrefined rare earth mixture (Mm — mischmetal) is very effective in lowering the cost of $MmNi_5$-based alloys. In recent works, it has been shown that electrochemical stability can also be improved by using non-stoichiometric compounds with a composition of $AB_{5\pm x}$.

Conventionally, the metal hydride materials have been prepared by arc melting and annealing. Non-equilibrium processing techniques such as mechanical alloying (MA), high-energy ball-milling (HEBM) or reactive milling

*Corresponding author. Fax: +48-61-665-3576.
E-mail address: jurczyk@sol.put.poznan.pl (M. Jurczyk).

0925-8388/00/$ – see front matter
PII: S0925-8388(00)01126-9

(mechanically induced gas–solid reactions) can be utilised to synthesise highly activated nanocrystalline powders [8,10–13]. Proper engineering of microstructure and surface by using unconventional processing techniques will lead to advanced nanocrystalline intermetallics representing a new generation of metal hydride materials with the following characteristics:

- high storage capacity,
- stable temperature–pressure cycling capacity during the life-time of the system,
- good corrosion stability,
- low costs.

The generation of metastable materials with an amorphous grain boundary phase offer a wider distribution of available sites for hydrogen and thus a totally different hydrogenation behaviour. The mechanism of amorphous phase formation by MA is due to a chemical solid state reaction, which is believed to be caused by the formation of a multilayer structure during milling [14]. Nanocrystalline hydrides show substantially enhanced absorption characteristics superior to that of the conventionally prepared materials [10,15].

In this work, the electrochemical properties of nanocrystalline $MmNi_{3.5}Al_{0.8}Co_{0.7}$ alloy, which has the hexagonal $CaCu_5$ structure, were investigated. The alloy synthesized by mechanical alloying was used us negative electrode for Ni–MH_x battery. The electrochemical properties of an amorphous and nanocrystalline powders were measured and compared with the polycrystalline material (powder $\leq$45 μm).

2. Experimental details

2.1. Preparation of the alloys and electrodes

Two different methods, arc melting and mechanical alloying, were used for preparation of the $MmNi_{3.5}Al_{0.8}Co_{0.7}$ alloy. Conventionally the material was prepared by arc melting stoichiometric amounts of the constituent elements (purity 99.8% or better) in an argon atmosphere. Mm denotes Ce-rich mischmetal with purity of 99%, which comprises of 31 wt% Ce, 25 wt% La, 21 wt% Nd, 14 wt% Sm, 8 wt% Pr and 1 wt% impurity. The as-cast ingot was homogenized at 1223 K for several days and then rapidly cooled to room temperature in water. The alloy lump was pulverized in few hydriding–dehydriding cycles to a fine powder ($\leq$45 μm).

Another processing method, mechanical alloying, was performed under argon atmosphere using a SPEX 8000 Mixer Mill. The round bottom stainless steel vial, which was equipped with a connection valve for evacuation or introduction of argon, was degassed for 12 h below 0.01 Pa. Then high purity argon was introduced into it, the pressure of which was up to 150 kPa. The purity of the starting materials was at least 99.8% and the composition of the starting powder mixture corresponded to the stoichiometry of the 'ideal' reactions, with an extra 8 wt% of mischmetal. The elemental powders (Mm$\leq$0.2 mm, Al 1–5 μm, Ni 3–7 μm and Co 149 μm) were mixed and poured into the vial. Mm powder was produced by filling the bulk material in an argon filled glove box (less than 5 ppm O_2). The mill was run up to 30-h for every powder preparation. The as-milled powders were heat treated at 1020 K for 0.5 h under high purity argon to form the hexagonal $CaCu_5$ phase. The powders were characterized by means of X-ray diffraction (XRD), transmission electron microscopy (TEM), scanning electron microscopy (SEM), and differential scanning calorimeter (DSC) measurements. XRD was performed using X-ray powder diffractometer with Co Kα radiation, at the various stages during milling, prior to annealing and after annealing. TEM and SEM were performed with a Philips EM300 and Jeol JSM-50A, respectively. To prepare the TEM specimens, the alloy powders were first rolled between Al plates, mechanically polished to thin films of thickness of 50 μm and ion milled. The crystallization behaviour of the mechanically alloyed powders was examined by differential scanning calorimetry (DSC 404, Netzsch) at a heating rate of 20 K min^{-1}. The pure argon purge was used to avoid oxidation. The crystallite sizes were estimated by the Scherrer method.

The mechanically alloyed $MmNi_{3.5}Al_{0.8}Co_{0.7}$ material, in both amorphous and in nanocrystalline forms, as well as the conventionally prepared material (pulverized to a fine powder), with 10 wt% addition of Ni powder, were subjected to electrochemical measurements as working electrodes after pressing (under 80 kN cm^{-2}) to 0.5 g pellet form between nickel nets acting as current collector. The diameter of each electrode was 10.4 mm and a thickness of approximately 1.4 mm. Soaking of the electrodes in 12 M KOH solution for 1 h at room temperature, with additional etching at 373 K for 10 min in the same solution, was sufficient for the initial activation.

2.2. Electrochemical measurements

The electrochemical properties of electrodes were measured in a three-compartment glass cell, using a much larger $NiOOH/Ni(OH)_2$ counter electrode and a Hg/HgO/6 M KOH reference electrode. All electrochemical measurements were carried out in deairated 6 M KOH solution prepared from Analar grade KOH and 18 MΩ cm^{-1} water, at 293 K. Potentiodynamic and galvanostatic techniques with either short or long-term pulses using a conventional apparatus were applied to study the charge–discharge kinetics of the electrodes. A detailed description of the electrochemical measurements was given in Ref. [9].

In the measurements of the electrochemical pressure-composition (e.p.c.) isotherm, after ten continuous charge–

discharge cycles, the electrode was intermittently charged and discharged under galvanostatic conditions with the resting periods (0.5 h) on open circuit long enough for the potential to equilibriate. The capacity obtained during the discharge was used to calculate the amount of hydrogen absorbed in one mole of the electrode material. Hydrogen pressure-composition (p.c.) isotherms for hydrogen absorption–desorption from the gas phase were obtained with a Sieverts type apparatus [16].

3. Results and discussion

The behaviour of MA process has been studied by X-ray diffraction, microstructural investigations as well as by electrochemical measurements. Fig. 1 shows a series of XRD spectra of mechanically alloyed Mm–Ni–Al–Co powder mixture (34.84 wt% Mm + 49.90 wt% Ni + 10.02 wt% Al + 5.24 wt% Co) subjected to milling for increasing time. The originally sharp diffraction lines of Mm, Ni, Al, Co (Fig. 1a) gradually become broader and their intensity decreases with milling time. The powder mixture milled for more than 30 h has transformed absolutely to the amorphous phase (Fig. 1b). It is worth noting that before amorphization, no shift of the diffraction lines was observed. This result means that the amorphous phase forms directly from the starting mixture of the elements (Mm, Ni, Al and Co), without formation of other phases. Using the Mm–Ni–Al–Co mixture composition as the representative material example, the behaviour of the grain size of the crystallites has been studied during the mechanical alloying process. The Ni (111) diffraction line remains visible up to 15 h of milling. This allows an estimation of the change in the crystalline size of Ni with increasing of the milling time. The final size of the crystallites, about 45 nm, seems to be favourable to the formation of an amorphous phase which develops at the Mm/Ni/Al/Co interfaces. Formation of alloy with hexagonal $CaCu_5$ type structure was achieved by annealing the amorphous material in high purity argon atmosphere at 1020 K for 0.5 h (Fig. 1c). Inevitably annealing results in grain growth, as was observed earlier in the case of other nanocomposite materials [17]. Table 1 reports the cell parameters of the studied materials along with the data obtained for the alloy samples hydrogenated from the gas phase.

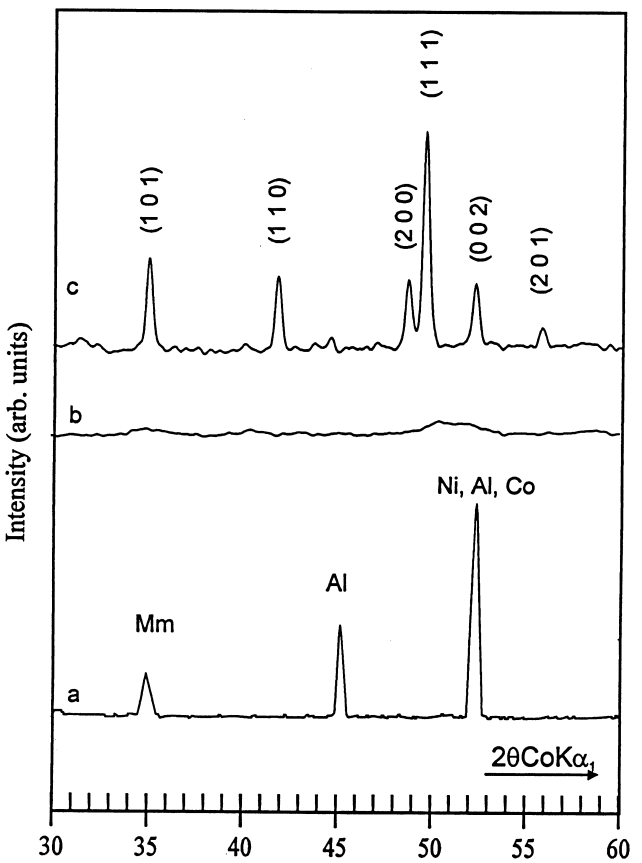

Fig. 1. XRD spectra of a mixture of Mm, Ni, Al and Co powders mechanically alloyed for different times in an argon atmosphere: (a) initial state (elemental powder mixture), (b) after MA for 30 h and (c) heat treated at 1020 K for 0.5 h.

The SEM technique was used to follow the changes in size and shape of the mechanically alloyed Mm–Ni–Al–Co powder mixture as a function of milling time. The microstructure that forms during MA consists of layers of the starting material. The thickness of the material decreases with increase in mechanical alloying time leading to true alloy formation [18]. The sample shows cleavage fracture morphology and inhomogeneous size distribution. The average crystallite sizes of MA $MmNi_{3.5}Al_{0.8}Co_{0.7}$ material were of the order of 50 nm and they have a tendency to agglomerate.

Using $MmNi_{4.2}Al_{0.8}$ as a representative alloy example, the amorphization process was also examined (Fig. 2). After mechanical alloying the DSC curve stabilized exhibiting one exothermic effect at 598 K for Mm–Ni–Al mixture. Taking into account the XRD results, one can assume that this effect is attributed to the crystallization of the amorphous phase formed by MA process. Microstructural investigation by TEM is shown in Fig. 3. The mechanically alloyed and annealed $MmNi_{4.2}Al_{0.8}$ material has nanocrystalline microstructure with grain size ~50 nm. This result is in agreement with XRD as well as SEM results.

Table 1
Structure parameters of $MmNi_{3.5}Al_{0.8}Co_{0.7}$ (A) and $MmNi_{3.5}Al_{0.8}Co_{0.7}H_x$ (A) prepared by different methods (see text for details)

Preparation method	Composition	a (Å)	c (Å)	V (Å^3)	ΔV (%)
Arc-melting	A	5.060	4.016	89.1	–
	B	5.422	4.267	108.6	22
Mechanical alloying and annealing	A	5.058	4.015	89.0	–
	B	5.416	4.237	107.6	21

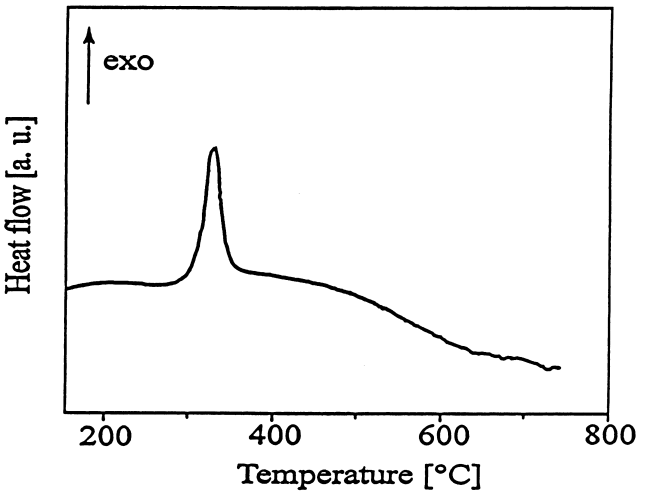

Fig. 2. DSC curve for amorphous Mm–Ni–Al mixture after 30 h mechanical alloying (heating rate in argon: 20 K min^{-1}).

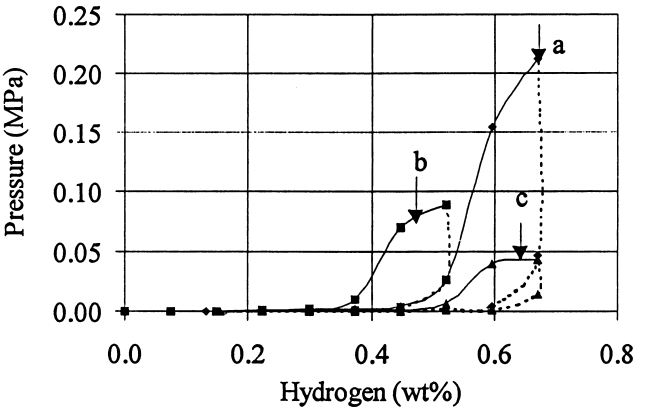

Fig. 4. Electrochemical pressure-composition isotherm for absorption (solid line) and desorption (dashed line) of hydrogen on: (a) polycrystalline, (b) amorphous and (c) nanocrystalline $MmNi_{3.5}Al_{0.8}Co_{0.7}$, at 293 K.

The electrochemical pressure-composition (e.p.c.) isotherms for absorption and desorption of hydrogen were obtained from the equilibrium potential values of the electrodes, measured during an intermittent charge and/or discharge cycles at constant current density, by using the Nernst equation according to the procedure reported by Balej [19]. The e.p.c. isotherms determined on the studied materials are illustrated in Fig. 4. Due to the amorphous nature of the $MmNi_{3.5}Al_{0.8}Co_{0.7}$ alloy prior to annealing (curve b) in Fig. 4), the hydrogen absorption–desorption characteristics are not satisfactory. Annealing causes transformation from the amorphous to the crystalline structure and produces grain boundaries. Anani et al. [8] noted, that grain boundaries are necessary for the migration of the hydrogen into the alloy. It is worth noting from Fig. 4, that the characteristics for polycrystalline and nanocrystalline materials are very similar with respect to hydrogen contents, but there is a small difference in the plateau pressures.

For the comparison, Fig. 5 shows the storage capacity of polycrystalline, amorphous and nanocrystalline $MmNi_{3.5}Al_{0.8}Co_{0.7}$ materials for the hydrogen desorption from the gas phase at 293 K, as characterized by equilibrium hydrogen pressure against hydrogen content isotherms (p.c.) measured using a Sieverts type equipment. One can note from this figure, that the characteristics are not similar. A progressive change of the pressure-composition isotherms is observed with annealing of an amorphous $MmNi_{3.5}Al_{0.8}Co_{0.7}$ material (Fig. 5b). After annealing at 1020 K for 0.5 h, a plateau is measured (Fig. 5c). This change is a result of relaxation as well as grain

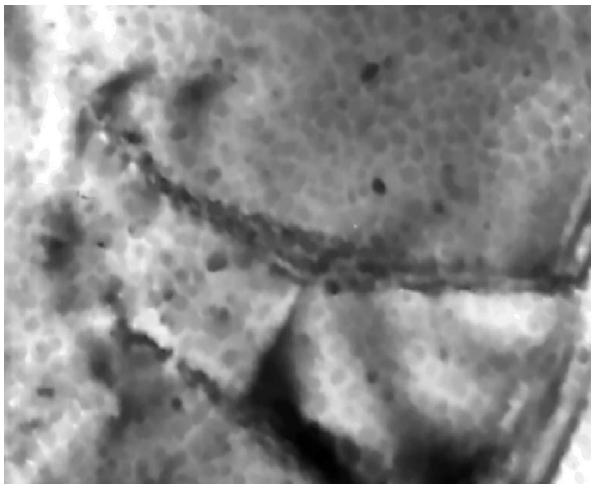

Fig. 3. TEM micrograph of nanocrystalline $MmNi_{4.2}Al_{0.8}$ sample, bright field image (magnification×32.000); note that grain boundaries of Al are also visible (see text).

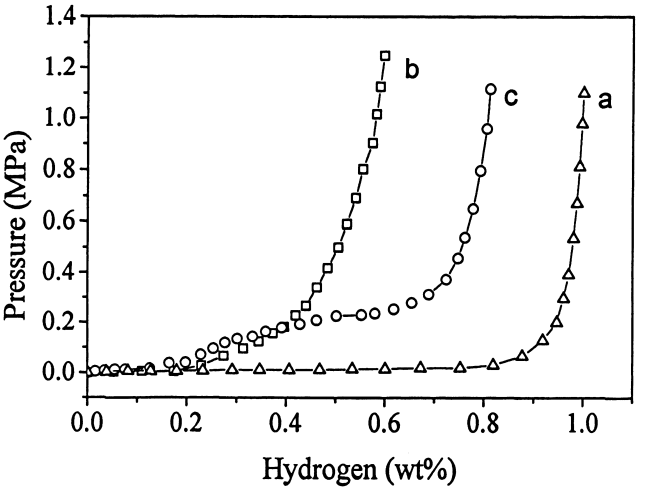

Fig. 5. Pressure composition isotherm for desorption of hydrogen from the gas phase on: (a) polycrystalline, (b) amorphous and (c) nanocrystalline $MmNi_{3.5}Al_{0.8}Co_{0.7}$, at 293 K.

growth. The isotherms of nanocrystalline (Fig. 5, curve c) material differ significantly from the polycrystalline material (Fig. 5, curve a), for which enhancement of solid state solubility was observed. It can be seen that the amount of absorbed hydrogen at a pressure of 1.2 MPa decreases for nanocrystalline material. Furthermore, the plateau pressure was found to increase for nanocrystalline material. The mechanical alloying process introduced into the material a significant amount of strain, chemical disorder and defects [10,15].

Recently, we have studied by X-ray photoelectron spectroscopy (XPS) the surface chemical composition and the cleanness of nanocrystalline La(Ni,Al,Co)$_5$-type alloys [20]. Results showed that the surface segregation under UHV conditions of lanthanum atoms in the MA nanocrystalline $LaNi_5$-type alloys is significantly stronger compared to that of polycrystalline powders from arc-melted ingots. This phenomena could considerably influence the hydrogenation process in such a type of materials. On the other hand, a small amount of the Fe impurities could be responsible for the observed, in this work, lower hydrogen storage capacity of the MA nanocrystalline $MmNi_{4.2}Al_{0.8}$ alloy compared to that of the polycrystalline sample. The level of oxygen impurities trapped in the mechanically alloyed powder during the processing is practically the same as in the arc-melted ingots.

From Figs. 4 and 5 it is apparent that for similar pressure (0.2 MPa) the chemical and electrochemical uptakes of hydrogen in nanocrystalline material are about equal (~0.68 wt%). On the other hand, the electrochemical capacities of the studied polycrystalline electrodes are smaller. These results point to differences in the surface state of alloy particles in the electrode material in an alkaline solution and in the hydrogen gas atmosphere. Generally, the electrochemical oxidation of particle surfaces in an alkaline solution, along with formation of a passive layer, inhibits the hydrogen electrosorption into the studied electrode materials. This is believed to be induced by the formation of an oxide layer (Mm_2O_3–$Mm(OH)_3$) on the electrode surface during the cycle test, which prevented hydrogen from penetrating the surface of the electrode [21,22].

Typical galvanostatic discharge curves of the electrodes fabricated from the polycrystalline, amorphous and nanocrystalline $MmNi_{3.5}Al_{0.8}Co_{0.7}$ materials are shown in Fig. 6. It can be seen, that the discharge capacities of polycrystalline as well as nanocrystalline electrodes are almost the same. As shown in this figure, the galvanostatic discharge characteristics of the Ni–MH_x battery with an amorphous material as the negative electrode are clearly lower. Fig. 7 shows the discharge capacities of the electrodes as a function of charge–discharge cycling number. It is worth noting, that annealed nanocrystalline $MmNi_{3.5}Al_{0.8}Co_{0.7}$ powder has greater capacities than the amorphous parent alloy powder. This improvement is due

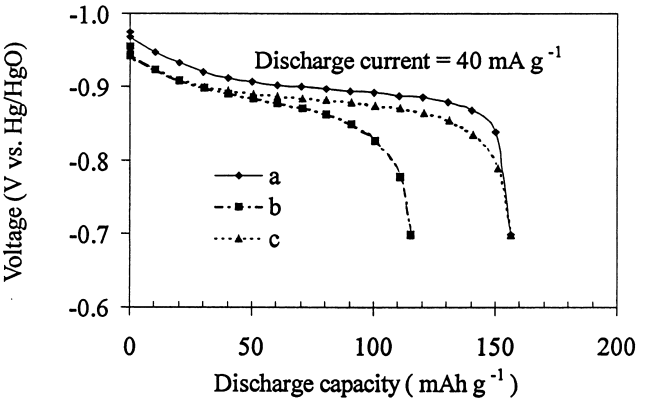

Fig. 6. Discharge curves of (a) polycrystalline, (b) amorphous and (c) nanocrystalline $MmNi_{3.5}Al_{0.8}Co_{0.7}$ electrodes, at 7th cycle (current density of 40 mA g^{-1} in 6 M KOH).

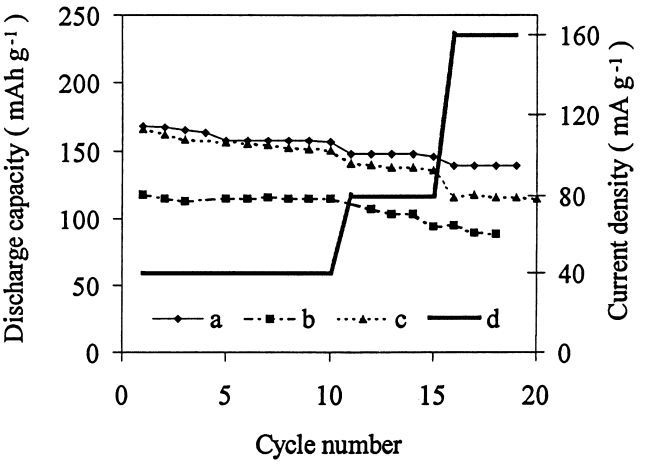

Fig. 7. Discharge capacity as a function of cycle numbers of electrode prepared with (a) polycrystalline, (b) amorphous and (c) nanocrystalline $MmNi_{3.5}Al_{0.8}Co_{0.7}$ (solution, 6 M KOH; temperature, 293 K). The charge conditions were: 40 mA g^{-1}; The discharge conditions were plotted on figure (d); cut-off potential vs. Hg/HgO/6 M KOH was of −0.7 V.

to a well-established diffusion path for hydrogen atoms along the numerous grain boundaries [10,23]. Table 2 reports the discharge capacities of the studied materials. It was found that the electrodes prepared with the nanocrystalline powders had slightly lower discharge

Table 2
Discharge capacities of $MmNi_{3.5}Al_{0.8}Co_{0.7}$ material prepared by arc melting and mechanical alloying and annealing at 10th cycle (current density of charging and discharging was 40 mA g^{-1})

Preparation method	Structure type	Discharge capacity at 10 cycle (mA h g^{-1})
Arc-melting	polycrystalline ($CaCu_5$)	157
Mechanical alloying	amorphous	115
Mechanical alloying and annealing	nanocrystalline ($CaCu_5$)	150

capacities, compared with a negative electrode prepared from polycrystalline $MmNi_{3.5}Al_{0.8}Co_{0.7}$ material.

4. Conclusion

In conclusion, nanocrystalline $MmNi_{3.5}Al_{0.8}Co_{0.7}$ alloy synthesized by mechanical alloying was used as negative electrode materials for a Ni–MH_x battery. The amorphous phase forms directly from the starting mixture of the elements, without other phase formation. Heating the MA samples at 1020 K for 0.5 h resulted in the formation of an ordered $CaCu_5$-type alloy. It was found that the electrodes prepared from the nanocrystalline powders had a slightly lower discharge capacity, compared with the negative electrode prepared from polycrystalline powder. The average crystallite sizes of MA $MmNi_{3.5}Al_{0.8}Co_{0.7}$ material were of the order of 50 nm. The properties of nanocrystalline electrode were attributed to the structural characteristics of the compound caused by mechanical alloying. Mechanical alloying is a suitable procedure for obtaining nanocrystalline $MmNi_5$-type materials.

References

[1] J.H.N. van Vucht, F.A. Kuijpers, H.C.A.M. Bruning, Philips Res. Rep. (1970) 133.
[2] H.H. van Mal, K.H.J. Buschow, A.R. Miedema, J. Less-Common Met. 35 (1974) 65.
[3] K.H.J. Buschow, P.C.P. Bouten, A.R. Miedema, Rep. Prog. Phys. 45 (1982) 937.
[4] S. Wakao, Y. Yonemura, H. Nakano, H. Shimada, J. Less-Common Met. 104 (1984) 365.
[5] S. Wakao, H. Sawa, J. Less-Common Met. 131 (1987) 31.
[6] G. Sandrock, S. Suda, L. Schlapbach, in: L. Schlapbach (Ed.), Hydrogen in Intermetallic Compounds II, Topics in Applied Physics, Vol. 67, Springer-Verlag, 1992, Chapter 5.
[7] Z. Yunshi, C. Youxiao, C. Jun, in: C. Shi, H. Li, A. Scott (Eds.), The First Pacific Rim International Conference on Advanced Materials and Processing (PRICM-1), The Minerals, Metals & Materials Society, 1992, pp. 1031–1033.
[8] A. Anani, A. Visintin, K. Petrov, S. Srinivasan, J.J. Reilly, J.R. Johnson, R.B. Schwarz, P.B. Desch, J. Power Sources 47 (1994) 261.
[9] M. Kopczyk, G. Wojcik, G. Mlynarek, A. Sierczynska, M. Beltowska-Brzezinska, J. Appl. Electrochem. 26 (1996) 639.
[10] L. Zaluski, A. Zaluska, J.O. Ström-Olsen, J. Alloys Comp. 253–254 (1997) 70.
[11] M. Au, F. Pourarian, S. Simizu, S.G. Sankar, L. Zhang, J. Alloys Comp. 223 (1995) 1.
[12] M. Jurczyk, W. Rajewski, W. Majchrzycki, G. Wojcik, J. Alloys Comp. 274 (1998) 299.
[13] M. Jurczyk, W. Rajewski, G. Wojcik, W. Majchrzycki, J. Alloys Comp. 285 (1999) 250.
[14] H. Gleiter, Progr. Mater. Sci. 33 (1989) 223.
[15] P. Tessier, L. Zaluski, A. Zaluska, J.O. Ström-Olsen, R. Schultz, Mater. Sci. Forum 225–227 (1996) 869.
[16] A. Sievert, A. Gatta, Z. Anorg. Chem. 172 (1928) 1.
[17] M. Jurczyk, S.J. Collocot, J.B. Dunlop, P.B. Gwan, J. Phys. D: Appl. Phys. 29 (1996) 2284.
[18] J.S. Benjamin, Materials Science Forum 88–90 (1992) 1.
[19] J. Balej, Inter. J. Hydrogen Energy 10 (1985) 363.
[20] L. Smardz, K. Smardz, M. Jurczyk, J. Jakubowicz, J. Alloys Comp. (submitted for publication).
[21] X.L. Wang, S. Suda, J. Alloys Comp. 194 (1993) 73.
[22] F. Liu, S. Suda, J. Alloys Comp. 232 (1996) 204.
[23] H. Kronberger, J. Alloys Comp. 253–254 (1997) 87.